NUMERICAL LINEAR ALGEBRA WITH APPLICATIONS
Numer. Linear Algebra Appl. 2006; **13**:677–697
Published online 19 June 2006 in Wiley InterScience (www.interscience.wiley.com). DOI: 10.1002/nla.492

Characteristic-mixed covolume methods for advection-dominated diffusion problems

Zhangxin Chen[1, 2, *, †], So-Hsiang Chou[3, ‡] and Do Young Kwak[4, §, ¶]

[1]*Research Center for Science, Xi'an Jiaotong University, Xi'an 710049, China*
[2]*Department of Mathematics, Box 750156, Southern Methodist University, Dallas, TX 75275-0156, U.S.A.*
[3]*Department of Mathematics and Statistics, Bowling Green State University, Bowling Green, OH 43403, U.S.A.*
[4]*Department of Mathematics, Korea Advanced Institute of Science and Technology, Taejon 305-701, Korea.*

SUMMARY

Characteristic-mixed covolume methods for time-dependent advection-dominated diffusion problems are developed and studied. The diffusion term in these problems is discretized using covolume methods applied to the mixed formulation of the problems on quadrilaterals, and the temporal differentiation and advection terms are treated by characteristic tracking schemes. Three characteristic tracking schemes are studied in the context of mixed covolume methods: the modified method of characteristics, the modified method of characteristics with adjusted advection, and the Eulerian–Lagrangian localized adjoint method. The proposed methods preserve the conceptual and computational merits of both characteristics-based schemes and the mixed covolume methods. Existence and uniqueness of a solution to the discrete problem arising from the methods is shown. Stability and convergence properties of these methods are also obtained; unconditionally stable results and error estimates of optimal order are established. Copyright © 2006 John Wiley & Sons, Ltd.

Received 23 December 2005; Revised 3 May 2006; Accepted 6 May 2006

KEY WORDS: characteristics-based method; covolume method; mixed finite element method; finite element method; control volume finite element method; control volume method; finite volume method; advection-dominated diffusion problem; stability; convergence; error estimate

*Correspondence to: Zhangxin Chen, Department of Mathematics, Box 750156, Southern Methodist University, Dallas, TX 75275-0156, U.S.A.
†E-mail: zchen@mail.smu.edu
‡E-mail: chou@bgnet.bgsu.edu
§E-mail: kdy@kaist.ac.kr
¶This paper is dedicated to Professor Richard E. Ewing on the occasion of his 60th birthday.

1. INTRODUCTION

Consider the time-dependent advection-dominated diffusion problem on a bounded polygonal domain $\Omega \subset \mathbb{R}^2$ with boundary Γ for the unknown solution p:

$$\frac{\partial(cp)}{\partial t} + \nabla \cdot (\mathbf{b}p - \mathbf{a}\nabla p) + Rp = f \tag{1}$$

where c, $\mathbf{b}$ (vector), $\mathbf{a}$ (tensor), R, and f are given functions. This problem involves advection ($\mathbf{b}$), diffusion ($\mathbf{a}$), reaction (R), and accumulation (c). Many problems arise in form (1), such as transport problems for multiphase flow in porous media and density problems for semiconductor modelling [1]. When diffusion dominates advection, finite element approximation methods that involve a backward Euler scheme for the accumulation term produce satisfactory numerical solutions for (1). When advection dominates diffusion, however, these methods may not perform well. In particular, they exhibit excessive non-physical oscillations when the solution to (1) is not smooth. Standard upstream weighting approaches have been applied to finite difference and finite element methods with the purpose of eliminating the non-physical oscillations, but these approaches significantly smear sharp fronts of the solution and suffer from grid-orientation difficulties. While extremely fine mesh refinement is possible to overcome these drawbacks, it is not feasible because of the excessive computational effort involved (particularly in multiple dimensions).

Many numerical techniques have been proposed to avoid the non-physical oscillations when advection dominates, such as the optimal spatial technique. This technique employs an Eulerian approach based on the minimization of the error in the approximation of spatial derivatives and the use of optimal test functions satisfying a local adjoint problem [2, 3]. It produces an upstream bias in the resulting approximation and has the numerical properties: (a) time truncation errors dominate the solution. (b) The solution has significant numerical diffusion and phase errors. (c) The Courant number (i.e. $|\mathbf{b}\Delta t/(ch)|$) is in general restricted to be smaller than one, where Δt and h are the temporal and spatial mesh sizes, respectively.

Other Eulerian techniques such as the Petrov–Galerkin finite element techniques have been proposed to employ non-zero spatial truncation errors to cancel temporal errors and thus reduce the overall truncation errors [4, 5]. Although these techniques improve accuracy in the approximation of the solution, they still suffer from the strict Courant number limitation mentioned above.

Another class of approximation techniques for the numerical solution of Equation (1) are the Eulerian–Lagrangian techniques. Because of the Lagrangian nature of advection in (1), these techniques treat the advection and accumulation by a characteristic tracking approach. The properties of this class include: (a) the Courant number restriction of the purely Eulerian techniques is alleviated because of the use of the characteristic tracking; (b) because the temporal and spatial dimensions are coupled via the characteristic tracking, the effect of time truncation errors present in optimal spatial techniques is significantly reduced; and (c) they yield non-oscillatory solutions without numerical diffusion, using reasonably large time steps on grids no finer than necessary to resolve the solution on the moving fronts [1]. The Eulerian–Lagrangian techniques have been applied in the context of finite element methods [6–10]. In this paper, we generalize these techniques to the setting of covolume methods applied to the mixed formulation of problem (1).

In some applications, such as those mentioned above, the vector variable $\mathbf{b}p - \mathbf{a}\nabla p$ is the primary variable in which one is interested. Standard mixed finite element methods were introduced to approximate both this vector and the scalar variable p simultaneously and to give a high-order approximation of both variables [1, 11]. On the other hand, mixed covolume methods have been

DOI: 10.1002/nla

developed with the same purpose, in addition to that they often produce smaller solution errors [12]. Unlike the mixed finite element methods that use a primary grid, the mixed covolume methods use a conservation law on a primary volume grid for the scalar variable and a constitutive law on a dual volume or covolume grid for the vector variable. Depending on how they are interpreted, these methods are referred to as mixed covolume methods (preferred by us), mixed control volume methods, and mixed balance methods [13–17]. Regardless of their physical interpretations, this class of numerical methods can mathematically be studied as Petrov–Galerkin methods with trial spaces associated with certain finite element spaces and test spaces related to finite volumes.

Covolume methods are particularly popular in computational fluid dynamics thanks to their local conservative properties [18, 19]. They generate the discrete counterpart of an underlying physical conservation law governing the behaviour of the fluid system. These methods were originally interpreted as finite difference methods on an irregular grid that compute only the normal components of the flux variable in fluid dynamics [19]. Only recently has Chou connected them to the mixed finite element framework of the Stokes equations [20].

In this paper we propose and analyse characteristic-mixed covolume methods for problem (1). That is, the diffusion term in (1) is discretized using mixed covolume methods, and the accumulation and advection terms are treated by characteristic tracking schemes. The proposed methods preserve the conceptual and computational merits of both characteristics-based schemes and the mixed covolume methods. For example, they can take reasonably large time steps, capture sharp solution fronts, have local conservative properties, and give high-order approximations to the flux variable. Three characteristic tracking schemes are analysed in the context of the mixed covolume methods: the modified method of characteristics (MMOC) [10, 21], the modified method of characteristics with adjusted advection (MMOCAA) [22], and the Eulerian–Lagrangian localized adjoint method (ELLAM) [7]. Existence and uniqueness of a solution to the discrete problem arising from the characteristic-mixed covolume methods is shown. Stability and convergence properties of these methods are also obtained; unconditionally stable results and error estimates of optimal order are established.

There has been a question unanswered for some time: Can the Eulerian–Lagrangian techniques be applied in the setting of mixed covolume methods? This question is valid in that covolumes are used in these methods and these covolumes can be overlapping. In this paper, we are able to answer this question thanks to the introduction of a critical mapping from the mixed finite element spaces for the vector variable to the test spaces used in the mixed covolume methods.

The rest of the paper is outlined as follows. The definition and analysis of three characteristic mixed covolume methods will be presented in the next three sections. The stability and convergence proof will be given in Section 5.

2. MMOC-MIXED COVOLUME METHODS

2.1. The continuous problem

To explain the idea of combining a characteristic method and mixed covolume methods, we first consider the MMOC [10, 21]. This characteristic method is easy to set up and implement, and is still in wide use. It is based on the non-divergence form of problem (1):

$$c(\mathbf{x})\frac{\partial p}{\partial t} + \mathbf{b}(\mathbf{x},t)\cdot\nabla p - \nabla\cdot(\mathbf{a}(\mathbf{x},t)\nabla p) + R(\mathbf{x},t)p = f(\mathbf{x},t), \quad \mathbf{x}\in\Omega, \quad t>0. \tag{2}$$

DOI: 10.1002/nla

To complete the definition of this problem, we need boundary and initial conditions. It is well known that the MMOC is not flexible in the treatment of general boundary conditions. Hence, to avoid the difficulty associated with the boundary conditions, we assume that (2) is Ω-periodic; i.e. Ω is a rectangle and all functions in (2) are spatially Ω-periodic. In fact, this is physically reasonable because no-flow boundaries are usually handled by reflection and interior flow behaviour is often much more important than boundary effects in fluid flow problems, for example. The treatment of general boundary conditions will be considered in the fourth section where an Eulerian–Lagrangian approach is adopted. The initial condition is

$$p(\mathbf{x}, 0) = p_0(\mathbf{x}), \quad \mathbf{x} \in \Omega \tag{3}$$

Let

$$\psi(\mathbf{x}, t) = (c^2(\mathbf{x}) + |\mathbf{b}(\mathbf{x}, t)|^2)^{1/2}$$

where $|\mathbf{b}|^2 = b_1^2 + b_2^2$ and $\mathbf{b} = (b_1, b_2)$. Throughout this paper, we assume that the accumulation and reaction coefficients, c and R, satisfy

$$c(\mathbf{x}) \geqslant c_* > 0, \quad R(\mathbf{x}, t) \geqslant 0, \quad \mathbf{x} \in \Omega, \quad t > 0 \tag{4a}$$

and the diffusion tensor $\mathbf{a} = (a_{ij})$ is bounded, symmetric, and uniformly positive-definite in $\mathbf{x}$ and t:

$$0 < a_* \leqslant |\boldsymbol{\eta}|^2 \sum_{i,j=1}^{2} a_{ij}(\mathbf{x}, t)\eta_i\eta_j \leqslant a^* < \infty, \quad \mathbf{x} \in \Omega, \quad \boldsymbol{\eta} \neq \mathbf{0} \in \mathbb{R}^2, \quad t > 0 \tag{4b}$$

where $\boldsymbol{\eta} = (\eta_1, \eta_2)$.

Let the characteristic direction corresponding to the hyperbolic part of (2), $c\partial p/\partial t + \mathbf{b} \cdot \nabla p$, be denoted by $\boldsymbol{\tau}$, so

$$\frac{\partial}{\partial \boldsymbol{\tau}} = \frac{c(\mathbf{x})}{\psi(\mathbf{x}, t)} \frac{\partial}{\partial t} + \frac{1}{\psi(\mathbf{x}, t)} \mathbf{b}(\mathbf{x}, t) \cdot \nabla$$

With this definition, we write (2) in the system of two first-order partial differential equations:

$$\begin{aligned} \psi(\mathbf{x}, t)\frac{\partial p}{\partial \boldsymbol{\tau}} + \nabla \cdot \mathbf{u} + R(\mathbf{x}, t)p = f(\mathbf{x}, t), \quad \mathbf{x} \in \Omega, \quad t > 0 \\ \mathbf{u} = -\mathbf{a}(\mathbf{x}, t)\nabla p, \quad \mathbf{x} \in \Omega, \quad t > 0 \end{aligned} \tag{5}$$

For $k \geqslant 0$, the standard Sobolev spaces $H^k(\Omega) = W^{k,2}(\Omega)$ are used in this paper, with the usual norms. For $k = 0$, set $L^2(\Omega) = H^0(\Omega)$. In addition, we define the linear space

$$\mathbf{H}(\text{div}, \Omega) = \{\mathbf{v} = (v_1, v_2) \in (L^2(\Omega))^2 : \nabla \cdot \mathbf{v} \in L^2(\Omega)\}$$

Furthermore, $\mathbf{H}_{\text{per}}(\text{div}, \Omega)$ and $L^2_{\text{per}}(\Omega)$ are defined as the closure of $C^\infty_{\text{per}}(\Omega)$ (the subset of $C^\infty(\mathbb{R}^2)$ of Ω-periodic functions) under the norms $\|\cdot\|_{\mathbf{H}(\text{div},\Omega)}$ and $\|\cdot\|_{L^2(\Omega)}$, respectively. Set

$$\mathbf{V} = \mathbf{H}_{\text{per}}(\text{div}, \Omega), \quad W = L^2_{\text{per}}(\Omega)$$

We use the inner product in $L^2(\Omega)$ or $(L^2(\Omega))^2$, as appropriate:

$$(v, w)_S = \int_S v(\mathbf{x})w(\mathbf{x})\, d\mathbf{x}$$

DOI: 10.1002/nla

If $S=\Omega$, we omit it in this notation. Now, applying Green's formula in space and the periodic boundary condition, (5) is recast in the equivalent mixed variational form

$$\begin{gathered}\left(\psi\frac{\partial p}{\partial \boldsymbol{\tau}}, w\right)+(\nabla\cdot\mathbf{u}, w)+(Rp, w)=(f, w), \quad w\in W,\ t>0\\ (\mathbf{a}^{-1}\mathbf{u}, \mathbf{v})-(\nabla\cdot\mathbf{v}, p)=0, \quad \mathbf{v}\in\mathbf{V},\ t>0\\ p(\mathbf{x}, 0)=p_0(\mathbf{x}), \quad \mathbf{x}\in\Omega\end{gathered} \tag{6}$$

2.2. MMOC-mixed covolume methods

Let $0=t^0<t^1<\cdots<t^n<\cdots$ be a partition in time, with $\Delta t^n=t^n-t^{n-1}$. For a generic function v of time, set $v^n=v(t^n)$. A characteristic is approximated by

$$\check{\mathbf{x}}_n=\mathbf{x}-\frac{\Delta t^n}{c(\mathbf{x})}\mathbf{b}(\mathbf{x}, t^n) \tag{7}$$

Furthermore, we see that, at $t=t^n$,

$$\begin{aligned}\psi\frac{\partial p}{\partial \boldsymbol{\tau}} &\approx \psi(\mathbf{x}, t^n)\frac{p(\mathbf{x}, t^n)-p(\check{\mathbf{x}}_n, t^{n-1})}{(|\mathbf{x}-\check{\mathbf{x}}_n|^2+(\Delta t^n)^2)^{1/2}}\\ &= c(\mathbf{x})\frac{p(\mathbf{x}, t^n)-p(\check{\mathbf{x}}_n, t^{n-1})}{\Delta t^n}\end{aligned} \tag{8}$$

That is, a backtracking scheme is used to approximate the characteristic derivative (see Figure 1).

Let K_h be a regular partition of Ω into non-overlapping (open) finite elements K:

$$\bar{\Omega}=\bigcup_{K\in K_h}\bar{K}$$

such that no vertex of one element lies in the interior of an edge of another element, where $\bar{\Omega}$ and $\bar{K}$ represent the closure of Ω and K (i.e. $\bar{\Omega}=\Omega\cup\Gamma$ and $\bar{K}=K\cup\partial K$), respectively. The mesh parameters h_K and h are defined as follows:

$$h_K=\operatorname{diam}(K) \quad \text{and} \quad h=\max_{K\in K_h} h_K$$

where $\operatorname{diam}(K)$ is the length of the longest edge of $\bar{K}$. Associated with K_h, let $\mathbf{V}_h\times W_h$ be a pair of standard mixed finite element spaces [23–28].

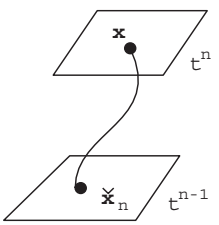

Figure 1. An illustration of the definition $\check{\mathbf{x}}_n$.

DOI: 10.1002/nla

Based on earlier results of Chou and Kwak [14, 20], a unified framework was presented for a number of mixed covolume methods [29]. This framework connects all these methods to the standard mixed finite element methods using an injective mapping γ_h from the space $\mathbf{V}_h$ to a test space $\mathbf{Y}_h$. Using this mapping, we define the MMOC-mixed covolume methods for (2): For $n = 1, 2, \ldots$, find $\mathbf{u}_h^n \in \mathbf{V}_h$ and $p_h^n \in W_h$ such that

$$\begin{gathered}\left(c\frac{p_h^n - \check{p}_h^{n-1}}{\Delta t^n}, w\right) + (\nabla \cdot \mathbf{u}_h^n, w) + (R^n p_h^n, w) = (f^n, w), \quad w \in W_h \\ ((\mathbf{a}^n)^{-1}\mathbf{u}_h^n, \gamma_h \mathbf{v}) - b(\gamma_h \mathbf{v}, p_h^n) = 0, \quad \mathbf{v} \in \mathbf{V}_h\end{gathered} \tag{9}$$

where the bilinear form $b(\cdot, \cdot)$ (as yet unspecified) is related to the divergence term and

$$\check{p}_h^{n-1} = p_h(\check{\mathbf{x}}_n, t^{n-1}) = p_h\left(\mathbf{x} - \frac{\Delta t^n}{c(\mathbf{x})}\mathbf{b}(\mathbf{x}, t^n), t^{n-1}\right) \tag{10}$$

The initial approximation p_h^0 can be defined as any reasonable approximation of p_0 in W_h such as its L^2-projection into W_h:

$$(p_h^0, w) = (p_0, w) \quad \forall w \in W_h \tag{11}$$

Comparing the mixed covolume methods in system (9) with the standard mixed finite element methods, one sees the presence of the operator γ_h in the former. This operator and the test space $\mathbf{Y}_h$ remain to be constructed. Their constructions are critical for the mixed covolume methods to produce optimal order convergence rates.

To prove the well-posedness of system (9), we make two hypotheses on γ_h:

$$b(\gamma_h \mathbf{v}, w) = (\nabla \cdot \mathbf{v}, w) \quad \forall \mathbf{v} \in \mathbf{V}_h, w \in W_h \tag{H1}$$

and there is a positive constant C_1 such that

$$(\mathbf{a}^{-1}\mathbf{v}, \gamma_h \mathbf{v}) \geqslant C_1 \|\mathbf{v}\|^2_{\mathbf{L}^2(\Omega)} \quad \forall \mathbf{v} \in \mathbf{V}_h \tag{H2}$$

Theorem 2.1
Under conditions (4), (H1), and (H2), system (9) has a unique solution.

Proof
Because (9) is a finite system, it suffices to show uniqueness of the solution. Setting $f = p_0 = 0$, it follows from (9) and (H1) that

$$\begin{gathered}\left(c\frac{p_h^n - \check{p}_h^{n-1}}{\Delta t^n}, w\right) + (\nabla \cdot \mathbf{u}_h^n, w) + (R^n p_h^n, w) = 0, \quad w \in W_h \\ ((\mathbf{a}^n)^{-1}\mathbf{u}_h^n, \gamma_h \mathbf{v}) - (\nabla \cdot \mathbf{v}, p_h^n) = 0, \quad \mathbf{v} \in \mathbf{V}_h\end{gathered}$$

We complete the proof by an induction argument. Note that $p_h^0 = 0$ via assumption. Let $p_h^{n-1} = 0$; the addition of the above two equations with $\mathbf{v} = \mathbf{u}_h^n$ and $w = p_h^n$ yields

$$\frac{1}{\Delta t^n}(cp_h^n, p_h^n) + ((\mathbf{a}^n)^{-1}\mathbf{u}_h^n, \gamma_h \mathbf{u}_h) + (R^n p_h^n, p_h^n) = 0$$

DOI: 10.1002/nla

which, together with (4) and (H2), implies

$$\mathbf{u}_h^n = \mathbf{0}, \quad p_h^n = 0$$

Thus the desired result follows. □

In addition to assumption (4), we assume that the accumulation and advection coefficients, c and $\mathbf{b}$, satisfy

$$c \in W^{1,\infty}(\Omega), \quad \mathbf{b} \in (L^\infty(J; W^{1,\infty}(\Omega)))^2 \tag{12}$$

where $J = (0, T]$ $(T > 0)$ is the time interval of interest.

Theorem 2.2
Under (4), (H1), (H2), and (12), the solution of system (9) satisfies the stability result

$$\|p_h\|_{L^\infty(J;L^2(\Omega))} + \|\mathbf{u}_h\|_{\mathbf{L}^2(\Omega_T)} \leqslant C(\|f\|_{L^2(\Omega_T)} + \|p_0\|_{L^2(\Omega)}) \tag{13}$$

where $\Omega_T = \Omega \times J$, and the constant C is independent of h, and

$$\|f\|_{L^2(\Omega_T)} = \left(\sum_{n=1}^{N} \|f^n\|_{L^2(\Omega)}^2 \Delta t^n \right)^{1/2}$$

This stability result will be proven in the fifth section.

2.3. Examples

As noted, the standard mixed finite element methods use a primary partition K_h, while the mixed covolume methods use K_h and a partition K_h' that is dual to K_h. The most well-known example is the MAC (marker and cell) method that employs two staggered rectangular grids [30]. These covolume methods can use either non-overlapping (see Figure 2) or overlapping (see Figure 3) covolumes. The left-hand figure in Figure 2 is a primary partition that consists of rectangles, and a typical interior covolume in its dual partition is the dashed quadrilateral, the union of two triangles $T_e^- \cup T_e^+$ with the common edge e in K_h. The two vertices inside the two rectangles are their centres. Note that each edge in K_h corresponds to a covolume. Near the boundary Γ a covolume is either T_e^- or T_e^+. The right-hand figure in Figure 2 has an analogous meaning when the primary partition K_h consists of triangles. On the other hand, the dashed covolumes in Figure 3 are overlapping. This type of staggered grid is used in the MAC method [30]. In this paper, as an example, we focus on overlapping covolumes because the overlapping case is more difficult to handle than the non-overlapping case [31]. Furthermore, we analyse the characteristic-mixed covolume methods

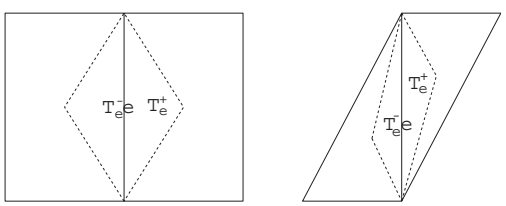

Figure 2. Primal and dual grids: $K_e' = T_e^- \cup e \cup T_e^+$.

DOI: 10.1002/nla

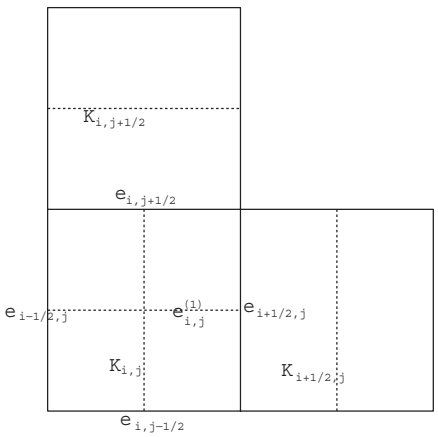

Figure 3. Dual grid with overlapping covolumes.

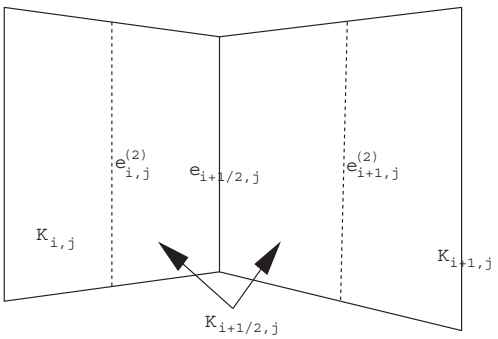

Figure 4. Primal and dual quadrilaterals.

on quadrilateral grids. Quadrilaterals can be regarded as logical rectangles or distorted rectangles (see Figure 4). They are harder to analyse than triangles and rectangles. Finite difference and mixed covolume methods over quadrilateral grids were considered in References [17, 31], respectively, and the standard mixed finite element methods over these grids were studied in References [32, 33]. The quadrilateral grids are particularly of interest in petroleum reservoir simulations [34].

2.3.1. Quadrilateral and dual grids. Let K_h be a partition of Ω into convex quadrilaterals. The partition is logically rectangular in the sense that each quadrilateral has a unique eastern, western, northern, and southern adjacent neighbours if they exist. Thus, each quadrilateral can be indexed by two indices: $K_h = \{K_{i,j}\}$ (see Figures 3 or 4). The eastern (respectively, northern) and western (respectively, southern) edges of K_{ij} are represented by

$$e_{i\pm 1/2,j} = \bar{K}_{i,j} \cap \bar{K}_{i\pm 1,j} \quad \text{(respectively, } e_{i,j\pm 1/2} = \bar{K}_{i,j} \cap \bar{K}_{i,j\pm 1}\text{)}$$

DOI: 10.1002/nla

In addition, the line segment joining the midpoints of $e_{i-1/2,j}$ and $e_{i+1/2,j}$ (respectively, $e_{i,j-1/2}$ and $e_{i,j+1/2}$) is indicated by $e_{i,j}^{(1)}$ (respectively, $e_{i,j}^{(2)}$). The covolume formed by the left-hand quadrilateral between the edges $e_{i,j}^{(2)}$ and $e_{i+1/2,j}$ and the right-hand quadrilateral between the edges $e_{i+1/2,j}$ and $e_{i+1,j}^{(2)}$ is $K_{i+1/2,j}$ (see Figure 4). The covolume $K_{i,j+1/2}$ is defined in an analogous manner.

Denote by T_i the subtriangle of $K \in K_h$ with vertices $\mathbf{m}_{i-1}$, $\mathbf{m}_i$, and $\mathbf{m}_{i+1}$, $i = 1, 2, 3, 4$, where $\mathbf{m}_0 = \mathbf{m}_4$. Define $\rho_K = 2 \min_{1 \leqslant i \leqslant 4}\{\text{diameter of the circle inscribed in } T_i\}$. As in the triangular case, the partition K_h is regular if

$$h_K \leqslant C_2 \rho_K \quad \forall K \in K_h$$

where the constant C_2 is independent of h.

The test function space $\mathbf{Y}_h$ will be defined through a Piola transformation $\mathscr{P}_K$ from the reference rectangle $\hat{K} = [0, 1] \times [0, 1]$ to all quadrilaterals $\{K\}$. The vertices of $\hat{K}$ in the $\hat{x}\hat{y}$-plane are

$$\hat{\mathbf{m}}_1 = (0, 0), \quad \hat{\mathbf{m}}_2 = (1, 0), \quad \hat{\mathbf{m}}_3 = (1, 1), \quad \hat{\mathbf{m}}_4 = (0, 1)$$

For any convex quadrilateral $K \in K_h$ with the vertices $\mathbf{m}_i$, $i = 1, 2, 3, 4$ (enumerated in the counterclockwise direction), the injective bilinear transformation

$$\mathbf{x} = \mathbf{F}_K(\hat{\mathbf{x}}) = \mathbf{m}_1 + \mathbf{m}_{21}\hat{x} + \mathbf{m}_{41}\hat{y} + \mathbf{m}_0\hat{x}\hat{y}, \quad \hat{\mathbf{x}} = (\hat{x}, \hat{y})$$

maps $\hat{K}$ onto K (see Figure 5), where $\mathbf{m}_{ij} = \mathbf{m}_i - \mathbf{m}_j$ and $\mathbf{m}_0 = \mathbf{m}_{12} + \mathbf{m}_{34}$. Note that

$$\mathbf{m}_i = \mathbf{F}_K(\hat{\mathbf{m}}_i), \quad i = 1, 2, 3, 4$$

Moreover, the Jacobian matrix $\mathbf{J}_K$ of $\mathbf{F}_K$ is

$$\mathbf{J}_K = \begin{pmatrix} \dfrac{\partial x}{\partial \hat{x}} & \dfrac{\partial x}{\partial \hat{y}} \\ \dfrac{\partial y}{\partial \hat{x}} & \dfrac{\partial y}{\partial \hat{y}} \end{pmatrix} = (\mathbf{m}_{21} + \mathbf{m}_0\hat{y}, \mathbf{m}_{41} + \mathbf{m}_0\hat{x})$$

The Piola transformation $\mathscr{P}_K$ is now defined by

$$\mathbf{v} = \mathscr{P}_K\hat{\mathbf{v}} \equiv \frac{1}{\det(\mathbf{J}_K)}\mathbf{J}_K\hat{\mathbf{v}} \circ \mathbf{F}_K^{-1}$$

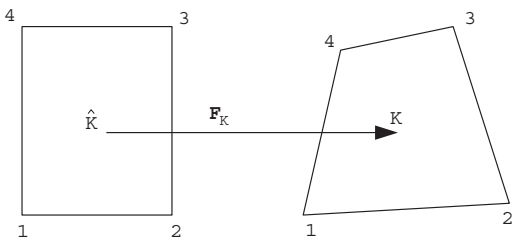

Figure 5. The bilinear transformation $\mathbf{F}_K$.

DOI: 10.1002/nla

where $\det(\mathbf{J}_K)$ is the determinant of $\mathbf{J}_K$. This transformation preserves the $\mathbf{H}(\mathrm{div})$ space on the reference rectangle $\hat{K}$ and has the properties [33]

$$\int_K \mathbf{v}\cdot\nabla w\,\mathrm{d}\mathbf{x} = \int_{\hat{K}} \hat{\mathbf{v}}\cdot\hat{\nabla}\hat{w}\,\mathrm{d}\hat{\mathbf{x}}, \quad \mathrm{div}\,\mathbf{v} = \frac{1}{\det(\mathbf{J}_K)}\hat{\mathrm{div}}\,\hat{\mathbf{v}}$$

where $\hat{w} = w\circ\mathbf{F}_K$.

2.3.2. Trial and test function spaces. As an example, we consider the Raviart–Thomas mixed finite element space of lowest order [28]. The scalar space W_h is simply the space of piecewise constants

$$W_h = \{w\in W : w|_K \text{ is constant, } K\in K_h\}$$

On the reference rectangle $\hat{K}$, $\mathbf{V}_h$ is

$$\mathbf{V}_h(\hat{K}) = \{\hat{\mathbf{v}} : \hat{\mathbf{v}} = (a+b\hat{x}, c+d\hat{y}),\ a,b,c,d\in\mathbb{R}\}$$

The space $\mathbf{V}_h$ over the quadrilateral grid K_h is defined through $\mathscr{P}_K$:

$$\mathbf{V}_h = \{\mathbf{v}\in\mathbf{V} : \mathbf{v}|_K = \mathscr{P}_K\hat{\mathbf{v}},\ \hat{\mathbf{v}}\in\mathbf{V}_h(\hat{K})\}$$

If $\boldsymbol{\nu}$ is the outward unit normal to an edge e of K, for $\hat{\mathbf{v}}\in\mathbf{V}_h(\hat{K})$ we see that

$$|e|\mathbf{v}\cdot\boldsymbol{\nu} = \hat{\mathbf{v}}\cdot\hat{\boldsymbol{\nu}}$$

where $|e|$ is the length of e and $\hat{\boldsymbol{\nu}}$ is the outward unit normal to the edge $\hat{e}$ corresponding to e. Consequently, every $\mathbf{v}\in\mathbf{V}_h$ has constant normal components on all edges in K_h, which can be used as degrees of freedom. Note that $\mathbf{v}$ is not a polynomial on K unless K is a parallelogram, and its divergence equals

$$\mathrm{div}\,\mathbf{v}|_K = \frac{1}{\det(\mathbf{J}_K)}\int_K \mathrm{div}\,\mathbf{v}\,\mathrm{d}\mathbf{x}$$

which does not belong to W_h.

The nodal basis functions of $\mathbf{V}_h(\hat{K})$ are

$$\hat{\boldsymbol{\varphi}}_{\hat{x},0} = \begin{pmatrix}1-\hat{x}\\ 0\end{pmatrix}, \quad \hat{\boldsymbol{\varphi}}_{\hat{x},1} = \begin{pmatrix}\hat{x}\\ 0\end{pmatrix}, \quad \hat{\boldsymbol{\varphi}}_{0,\hat{y}} = \begin{pmatrix}0\\ 1-\hat{y}\end{pmatrix}, \quad \hat{\boldsymbol{\varphi}}_{1,\hat{y}} = \begin{pmatrix}0\\ \hat{y}\end{pmatrix}$$

Then the basis of $\mathbf{V}_h$ is

$$\boldsymbol{\varphi}_{i+1/2,j} = \begin{cases}\mathscr{P}_{K_{i,j}}\hat{\boldsymbol{\varphi}}_{\hat{x},1} & \text{in } K_{i,j}\\ \mathscr{P}_{K_{i+1,j}}\hat{\boldsymbol{\varphi}}_{\hat{x},0} & \text{in } K_{i+1,j}\\ \mathbf{0} & \text{elsewhere}\end{cases} \tag{14}$$

DOI: 10.1002/nla

and

$$\boldsymbol{\varphi}_{i,j+1/2} = \begin{cases} \mathscr{P}_{K_{i,j}} \hat{\boldsymbol{\varphi}}_{1,\hat{y}} & \text{in } K_{i,j} \\ \mathscr{P}_{K_{i,j+1}} \hat{\boldsymbol{\varphi}}_{0,\hat{y}} & \text{in } K_{i,j+1} \\ \mathbf{0} & \text{elsewhere} \end{cases} \tag{15}$$

Note that $\boldsymbol{\varphi}_{i+1/2,j}$ has a unit flux on the edge $e_{i+1/2,j}$ and zero fluxes on other edges; $\boldsymbol{\varphi}_{i,j+1/2}$ has a similar meaning.

We are in a position to define the mapping $\gamma_h : \mathbf{V}_h \to \mathbf{Y}_h$, following Reference [31]. On the reference rectangle $\hat{K}$, $\hat{\gamma} : \mathbf{V}_h(\hat{K}) \to \mathbf{Y}_h(\hat{K})$ is defined by

$$\hat{\gamma}\hat{v}_1 = \begin{cases} \hat{v}_1(0, \hat{y}) & \text{on } [0, 1/2] \times [0, 1] \\ \hat{v}_1(1, \hat{y}) & \text{on } [1/2, 1] \times [0, 1] \end{cases}$$

and

$$\hat{\gamma}\hat{v}_2 = \begin{cases} \hat{v}_2(\hat{x}, 0) & \text{on } [0, 1] \times [0, 1/2] \\ \hat{v}_2(\hat{x}, 1) & \text{on } [0, 1] \times [1/2, 1] \end{cases}$$

where $\hat{\gamma}\hat{\mathbf{v}} = (\hat{\gamma}\hat{v}_1, \hat{\gamma}\hat{v}_2)^{\mathrm{T}}$ and $\hat{\mathbf{v}} = (\hat{v}_1, \hat{v}_2)^{\mathrm{T}}$ (the transpose). Now, for the basis of $\mathbf{V}_h$, it follows from the definition (14) that

$$\gamma_h \boldsymbol{\varphi}_{i+1/2,j} = \begin{cases} \mathscr{P}_{K_{i,j}}(1, 0)^{\mathrm{T}} & \text{on } \bar{K}_{i,j} \cap \bar{K}_{i+1/2,j} \\ \mathscr{P}_{K_{i+1,j}}(1, 0)^{\mathrm{T}} & \text{on } \bar{K}_{i+1/2,j} \cap \bar{K}_{i+1,j} \\ \mathbf{0} & \text{elsewhere} \end{cases}$$

Similarly, $\gamma_h \boldsymbol{\varphi}_{i,j+1/2}$ can be defined using (15). If $\mathbf{v} \in \mathbf{V}_h$ is represented by

$$\mathbf{v} = \sum_{i,j} (v_{i+1/2,j} \boldsymbol{\varphi}_{i+1/2,j} + v_{i,j+1/2} \boldsymbol{\varphi}_{i,j+1/2})$$

then we define

$$\gamma_h \mathbf{v} = \sum_{i,j} (v_{i+1/2,j} \gamma_h \boldsymbol{\varphi}_{i+1/2,j} + v_{i,j+1/2} \gamma_h \boldsymbol{\varphi}_{i,j+1/2})$$

Finally, $\mathbf{Y}_h$ is defined as the range space of γ_h, and the bilinear form $b(\cdot, \cdot)$ is defined as follows:

$$b(\gamma_h \mathbf{v}, w) = \sum_{i,j} (v_{i+1/2,j}[w_{i+1,j} - w_{i,j}] + v_{i,j+1/2}[w_{i,j+1} - w_{i,j}]), \quad \mathbf{v} \in \mathbf{V}_h,\ w \in W_h$$

where $w_{i,j} = w|_{K_{i,j}}$.

With the definition of γ_h and $b(\cdot, \cdot)$, hypothesis (H1) holds. Moreover, for sufficiently small $h > 0$, if assumption (4b) is satisfied, so is hypothesis (H2) [31]. Furthermore, the mapping γ_h has the properties

$$\|\gamma_h \mathbf{v}\|_{\mathbf{L}^2(\Omega)} \leqslant C \|\mathbf{v}\|_{\mathbf{L}^2(\Omega)}, \quad \mathbf{v} \in \mathbf{V}_h \tag{16}$$

DOI: 10.1002/nla

and

$$|(\mathbf{a}^{-1}\mathbf{w}, \mathbf{v} - \gamma_h \mathbf{v})| \leqslant Ch\|\mathbf{w}\|_{\mathbf{H}^1(\Omega)}\|\mathbf{v}\|_{\mathbf{L}^2(\Omega)}, \quad \mathbf{w} \in (H^1(\Omega))^2, \quad \mathbf{v} \in \mathbf{V}_h, \quad t>0 \tag{17}$$

where the C's are generic positive constants, independent of h.

The following error estimates will be proven in Section 5.

Theorem 2.3

Under assumptions (4) and (12), if $(\mathbf{u}, p)$ and $(\mathbf{u}_h, p_h)$ are the solutions to (6) and (9), respectively, then, for h sufficiently small,

$$\begin{aligned}
&\max_{1 \leqslant n \leqslant N} \|p^n - p_h^n\|_{L^2(\Omega)}^2 + \sum_{n=1}^{N} \|\mathbf{u}^n - \mathbf{u}_h^n\|_{\mathbf{L}^2(\Omega)}^2 \Delta t^n \\
&\quad \leqslant C \left(h \left[\|p\|_{L^\infty(J;H^1(\Omega))} + \|\mathbf{u}\|_{\mathbf{L}^2(J;H^1(\Omega))} + \left\| \frac{\partial p}{\partial t} \right\|_{L^2(J;H^1(\Omega))} \right.\right. \\
&\qquad \left.\left. + \left\| \frac{\partial p}{\partial \boldsymbol{\tau}} \right\|_{L^2(J;H^1(\Omega))} + \|p_0\|_{H^1(\Omega)} \right] + \Delta t \left\| \frac{\partial^2 p}{\partial \boldsymbol{\tau}^2} \right\|_{L^2(\Omega_T)} \right)
\end{aligned}$$

where we recall that $\boldsymbol{\tau}$ is the characteristic direction corresponding to the hyperbolic part of (2), $\Delta t = \max_{i=1,2,\ldots,N} \Delta t^n$, and $t^N = T$.

3. MMOCAA-MIXED COVOLUME METHODS

Problem (2) with the periodic boundary condition is considered in this section. Furthermore, to introduce the methods, we assume in this section that

$$\nabla \cdot \mathbf{b} = 0 \quad \text{in } \Omega, \ t>0 \tag{18}$$

That is, $\mathbf{b}$ is divergence free. This is physically reasonable since $\mathbf{b}$ is typically a velocity field and (18) corresponds to the incompressibility condition. Note that, by (18), the periodicity assumption, and the divergence theorem, Equation (2) with $R = 0$ and $f = 0$ yields the conservation law

$$\int_\Omega c(\mathbf{x}) p(\mathbf{x}, t)\, d\mathbf{x} = \int_\Omega c(\mathbf{x}) p_0(\mathbf{x})\, d\mathbf{x}, \quad t>0 \tag{19}$$

In real applications, it is desirable to maintain at least a discrete form of this law in any numerical approximation of (2). However, in general, (9) does not satisfy this property, and it creates an imbalance in mass. The imbalance stems from the advection (transport) process since the diffusion process in (9) has been shown to conserve mass locally [10]. To see this, set $\mathbf{a} = \mathbf{0}$, $R = f = 0$, and $w = 1$ in (9) to have

$$\int_\Omega c(\mathbf{x}) p_h^n(\mathbf{x})\, d\mathbf{x} = \int_\Omega c(\mathbf{x}) \check{p}_h^{n-1}(\mathbf{x})\, d\mathbf{x} \neq \int_\Omega c(\mathbf{x}) p_h^{n-1}(\mathbf{x})\, d\mathbf{x} \tag{20}$$

DOI: 10.1002/nla

Note that in the case where c is constant, preserving (19) requires that the Jacobian of the map (7) identically equal one. However, in general, if $\nabla \cdot (\mathbf{b}/c) \neq 0$, the Jacobian is $1 + O(\Delta t)$; it is $1 + O((\Delta t)^2)$ if (18) holds and c is constant Reference [1]. To preserve (19) numerically, we follow Reference [22] to use the modified method of characteristics with adjusted advection (MMOCAA).

Let W_h and p_h^0 be defined as in the previous section. For $1 \leqslant n \leqslant N$, given $p_h^{n-1} \in W_h$, set

$$Q_h^{n-1} = \int_\Omega c(\mathbf{x}) p_h^{n-1}(\mathbf{x})\, d\mathbf{x}, \quad \check{Q}_h^{n-1} = \int_\Omega c(\mathbf{x}) \check{p}_h^{n-1}(\mathbf{x})\, d\mathbf{x}$$

As mentioned above, $Q_h^{n-1} \neq \check{Q}_h^{n-1}$ in general. Define

$$\tilde{p}_h^{n-1}(\mathbf{x}) = \begin{cases} \max\{p_h^{n-1}(\tilde{\mathbf{x}}^-),\, p_h^{n-1}(\tilde{\mathbf{x}}^+)\} & \text{if } \check{Q}_h^{n-1} < Q_h^{n-1} \\ \min\{p_h^{n-1}(\tilde{\mathbf{x}}^-),\, p_h^{n-1}(\tilde{\mathbf{x}}^+)\} & \text{if } \check{Q}_h^{n-1} > Q_h^{n-1} \end{cases}$$

and

$$\tilde{Q}_h^{n-1} = \int_\Omega c(\mathbf{x}) \tilde{p}_h^{n-1}(\mathbf{x})\, d\mathbf{x}$$

where $\check{\mathbf{x}}$ is defined as in (7),

$$\tilde{\mathbf{x}}^- = \check{\mathbf{x}} - \gamma_1 \frac{b(\mathbf{x}, t^n)}{c(\mathbf{x})} (\Delta t^n)^2, \quad \tilde{\mathbf{x}}^+ = \check{\mathbf{x}} + \gamma_1 \frac{b(\mathbf{x}, t^n)}{c(\mathbf{x})} (\Delta t^n)^2$$

and γ_1 is a fixed positive constant (normally chosen to be less than one [22]). If $\check{Q}_h^{n-1} = \tilde{Q}_h^{n-1}$, we must accept that mass cannot be conserved; otherwise, find $\Lambda^{n-1} \in \mathbb{R}$ such that

$$Q_h^{n-1} = \Lambda^{n-1} \check{Q}_h^{n-1} + (1 - \Lambda^{n-1}) \tilde{Q}_h^{n-1} \tag{21}$$

Define

$$\hat{p}_h^{n-1} = \Lambda^{n-1} \check{p}_h^{n-1} + (1 - \Lambda^{n-1}) \tilde{p}_h^{n-1} \tag{22}$$

and

$$\hat{Q}_h^{n-1} = \int_\Omega c(\mathbf{x}) \hat{p}_h^{n-1}(\mathbf{x})\, d\mathbf{x}$$

Clearly, $\hat{Q}_h^{n-1} = Q_h^{n-1}$, so the conservation law is preserved. Now, continue in n with $\hat{p}_h^{n-1}$ in place of $\check{p}_h^{n-1}$ in the original procedure (9); i.e.

$$\begin{gathered} \left(c \frac{p_h^n - \hat{p}_h^{n-1}}{\Delta t^n}, w \right) + (\nabla \cdot \mathbf{u}_h^n, w) + (R^n p_h^n, w) = (f^n, w), \quad w \in W_h \\ ((\mathbf{a}^n)^{-1} \mathbf{u}_h^n, \boldsymbol{\gamma}_h \mathbf{v}) - b(\boldsymbol{\gamma}_h \mathbf{v}, p_h^n) = 0, \quad \mathbf{v} \in \mathbf{V}_h \end{gathered} \tag{23}$$

Note that Λ^{n-1} is bounded; $0 \leqslant \Lambda^{n-1} \leqslant 1$ for small Δt^{n-1} [22]. Theorems 2.1–2.3 remain valid for the MMOCAA-mixed covolume methods. In addition, the discussion on the examples given in Section 2.3 applies as well.

DOI: 10.1002/nla

4. EULERIAN–LAGRANGIAN MIXED COVOLUME METHODS

Periodic boundary conditions have been considered in the previous two sections. In this section, we consider an Eulerian–Lagrangian method, which is based on a space-time variational form and the divergence form of (2):

$$\begin{aligned} \frac{\partial(cp)}{\partial t} + \nabla\cdot(\mathbf{b}p - \mathbf{a}\nabla p) + Rp = f, \quad & \mathbf{x}\in\Omega, \ \ t>0 \\ (\mathbf{b}p - \mathbf{a}\nabla p)\cdot\boldsymbol{\nu} = g_-, \quad & \mathbf{x}\in\Gamma_-, \ \ t>0 \\ p = g_+, \quad & \mathbf{x}\in\Gamma_+, \ \ t>0 \\ p(\mathbf{x},0) = p_0(\mathbf{x}), \quad & \mathbf{x}\in\Omega \end{aligned} \tag{24}$$

where $\Omega\subset\mathbb{R}^2$ is a polygonal domain, the accumulation coefficient c can depend on time, $\boldsymbol{\nu}$ is the outward unit normal to Γ,

$$\Gamma_- = \{\mathbf{x}\in\Gamma : (\mathbf{b}\cdot\boldsymbol{\nu})(\mathbf{x})<0\}, \quad \Gamma_+ = \{\mathbf{x}\in\Gamma : (\mathbf{b}\cdot\boldsymbol{\nu})(\mathbf{x})\geqslant 0\}$$

and $g_-(\cdot,t)\in H^{-1/2}(\Gamma_-)$ and $g_+(\cdot,t)\in H^{1/2}(\Gamma_+)$ $(t\in J)$ are given functions. The boundaries Γ_- and Γ_+ are the inflow and outflow parts of Γ, respectively.

As in the previous two sections, for any $\mathbf{x}\in\Omega$ and two times $0\leqslant t^{n-1}<t^n$, the hyperbolic part of problem (24), $c\partial p/\partial t + \mathbf{b}\cdot\nabla p$, defines the characteristic $\check{\mathbf{x}}_n(\mathbf{x},t)$ along the interstitial velocity $\boldsymbol{\phi} = \mathbf{b}/c$:

$$\begin{aligned} \frac{\partial}{\partial t}\check{\mathbf{x}}_n &= \boldsymbol{\phi}(\check{\mathbf{x}}_n, t), \quad t\in J^n = [t^{n-1}, t^n) \\ \check{\mathbf{x}}_n(\mathbf{x}, t^n) &= \mathbf{x} \end{aligned} \tag{25}$$

In general, the characteristics in (25) can be determined only approximately. There are many ways to solve this first-order ordinary differential equation for approximate characteristics. We consider only an Euler method, as in the previous two sections.

The Euler method to solve (25) for the approximate characteristics is given: For any $\mathbf{x}\in\Omega$, we define

$$\check{\mathbf{x}}_n(\mathbf{x},t) = \mathbf{x} - \boldsymbol{\phi}(\mathbf{x},t^n)(t^n - t), \quad t\in[\check{t}(\mathbf{x}), t^n] \tag{26}$$

where $\check{t}(\mathbf{x}) = t^{n-1}$ if $\check{\mathbf{x}}_n(\mathbf{x},t)$ does not backtrack to the boundary Γ for $t\in[t^{n-1},t^n]$; $\check{t}(\mathbf{x})\in(t^{n-1},t^n]$ is the time instant when $\check{\mathbf{x}}_n(\mathbf{x},t)$ intersects Γ, i.e. $\check{\mathbf{x}}_n(\mathbf{x},\check{t}(\mathbf{x}))\in\Gamma$, otherwise. For $(\mathbf{x},t)\in\Gamma_+\times J^n$, the approximate characteristic emanating backward from $(\mathbf{x},t)$ is given by

$$\check{\mathbf{x}}_n(\mathbf{x},\theta) = \mathbf{x} - \boldsymbol{\phi}(\mathbf{x},t)(t-\theta), \quad \theta\in[\check{t}(\mathbf{x},t), t] \tag{27}$$

where $\check{t}(\mathbf{x},t) = t^{n-1}$ if $\check{\mathbf{x}}_n(\mathbf{x},\theta)$ does not backtrack to the boundary Γ for $\theta\in[t^{n-1},t]$; $\check{t}(\mathbf{x},t)\in(t^{n-1},t]$ is the time instant when $\check{\mathbf{x}}_n(\mathbf{x},\theta)$ intersects Γ otherwise. We have exploited a single step Euler method to determine the approximate characteristics from (25); a multi-step version can be also employed.

If Δt^n is sufficiently small (depending upon the smoothness of $\boldsymbol{\phi}$), the approximate characteristics do not cross each other, which is assumed. Then $\check{\mathbf{x}}_n(\cdot,t)$ is a one-to-one mapping of $\mathbb{R}^2$ to $\mathbb{R}^2$; we indicate its inverse by $\hat{\mathbf{x}}_n(\cdot,t)$.

DOI: 10.1002/nla

For any $t \in (t^{n-1}, t^n]$, we define

$$\tilde{\boldsymbol{\phi}}(\mathbf{x}, t) = \boldsymbol{\phi}(\hat{\mathbf{x}}_n(\mathbf{x}, t), t^n), \quad \tilde{\mathbf{b}} = \tilde{\boldsymbol{\phi}} c \tag{28}$$

We assume that $\tilde{\mathbf{b}} \cdot \boldsymbol{\nu} \geqslant 0$ on Γ_+.

Set

$$W = L^2(\Omega), \quad \mathbf{V} = \mathbf{H}(\mathrm{div}, \Omega) = \{\mathbf{v} \in (L^2(\Omega))^2 : \nabla \cdot \mathbf{v} \in L^2(\Omega)\}$$

The characteristic mixed variational form of (24) is [1]

$$\begin{aligned}
&(c^n p^n, v^n) - (c^{n-1} p^{n-1}, v^{n-1,+}) + (\Delta t^n R^n p^n, v^n) \\
&\quad - \sum_{K \in K_h} [(\Delta t^n \mathbf{u}^n \cdot \boldsymbol{\nu}_K, v^n)_{\partial K \setminus \Gamma_-} - (\Delta t^n \mathbf{u}^n, \nabla v^n)_K] \\
&= (\Delta t^n f^n, v^n) - \int_{J^n} \{(g_-, v)_{\Gamma_-} + (g_+ \tilde{\mathbf{b}} \cdot \boldsymbol{\nu}, v)_{\Gamma_+}\} \, \mathrm{d}t \\
&\quad + \int_{J^n} \{(\nabla \cdot [(\tilde{\mathbf{b}} - \mathbf{b}) p], v) - (p[\tilde{\mathbf{b}} - \mathbf{b}] \cdot \boldsymbol{\nu}, v)_{\Gamma_-}\} \, \mathrm{d}t \\
&(\mathbf{a}^{-1}\mathbf{u}, \mathbf{v}) + \sum_{K \in K_h} [(p, \mathbf{v} \cdot \boldsymbol{\nu}_K)_{K \setminus \Gamma_-} - (\nabla p, \mathbf{v})_K] = (g_+, \mathbf{v} \cdot \boldsymbol{\nu})_{\Gamma_+}, \quad \mathbf{v} \in \mathbf{V}, \ t > 0
\end{aligned} \tag{29}$$

where the test function $v(x, t)$ is assumed to be constant along the approximate characteristics $\check{\mathbf{x}}$, $v^{n-1,+} = v(x, t^{n-1,+}) = \lim_{\varepsilon \to 0^+} v(x, t^{n-1} + \varepsilon)$ to take account of the fact that $v(x, t)$ may be discontinuous at time levels, and $\Delta t^n(\mathbf{x}) = t^n - \check{t}(\mathbf{x})$.

Let K_h be a regular partition of Ω into convex quadrilaterals as in Section 2.3.1, and the spaces $\mathbf{V}_h \times W_h$ and the mapping $\gamma_h : \mathbf{V}_h \to \mathbf{Y}_h$ be defined as in Section 2.3.2. For any $w \in W_h$, we define a test function $v(\mathbf{x}, t)$ to be a constant extension of $w(\mathbf{x})$ into the space–time region $\Omega \times J^n$ along the approximate characteristics (refer to (26) and (27)):

$$\begin{aligned}
&v(\check{\mathbf{x}}_n(\mathbf{x}, t), t) = w(\mathbf{x}), \quad t \in [\check{t}(\mathbf{x}), t^n], \mathbf{x} \in \Omega \\
&v(\check{\mathbf{x}}_n(\mathbf{x}, \theta), \theta) = w(\mathbf{x}), \quad \theta \in [\check{t}(\mathbf{x}, t), t], (\mathbf{x}, t) \in \Gamma_+ \times J^n
\end{aligned} \tag{30}$$

Now, based on (29), the Eulerian–Lagrangian mixed covolume methods are defined: For $n = 1, 2, \ldots$, find $\mathbf{u}_h^n \in \mathbf{V}_h$ and $p_h^n \in W_h$ such that

$$\begin{aligned}
&(c^n p_h^n, v^n) - (c^{n-1} p_h^{n-1}, v^{n-1,+}) + (\Delta t^n R^n p_h^n, v^n) \\
&\quad - \sum_{K \in K_h} [(\Delta t^n \mathbf{u}_h^n \cdot \boldsymbol{\nu}_K, v^n)_{\partial K \setminus \Gamma_-} - (\Delta t^n \mathbf{u}_h^n \nabla v^n)_K] \\
&= (\Delta t^n f^n, v^n) - \int_{J^n} \{(g_-, v)_{\Gamma_-} + (g_+ \tilde{\mathbf{b}} \cdot \boldsymbol{\nu}, v)_{\Gamma_+}\} \, \mathrm{d}t \\
&(\Delta t^n (\mathbf{a}^n)^{-1} \mathbf{u}_h^n, \gamma_h \mathbf{v}) + \sum_{K \in K_h} [(\Delta t^n p_h^n, \mathbf{v} \cdot \boldsymbol{\nu}_K)_{K \setminus \Gamma_-} - (\Delta t^n \nabla p_h^n, \mathbf{v})_K] \\
&= \int_{J^n} (g_+^n, \mathbf{v} \cdot \boldsymbol{\nu})_{\Gamma_+} \, \mathrm{d}t
\end{aligned} \tag{31}$$

for $\mathbf{v} \in \mathbf{V}_h$, $w \in W_h$, and v the constant extension of w along the approximate characteristics.

DOI: 10.1002/nla

Note that the space W_h contains piecewise constants. If we take $w = 1$ on each element $K \in K_h$ in the first equation of (31), we see that mass is conserved locally up to the error in approximating the integrals involved. As a matter of fact, this equation expresses local conservation of mass where fluid is transported along the approximate characteristics.

Theorem 4.1
Under condition (4), system (31) has a unique solution.

The proof of this theorem can be completed in a similar fashion as for Theorem 2.1. We also have the next stability and convergence theorems whose proof will be carried out in Section 5.

Theorem 4.2
Under assumptions (4) and (12), the solution of system (9) satisfies the stability result

$$\|p_h\|_{L^\infty(J;L^2(\Omega))} + \|\mathbf{u}_h\|_{\mathbf{L}^2(\Omega_T)} \leqslant C(\|f\|_{L^2(\Omega_T)} + \|p_0\|_{L^2(\Omega)} + \|g_-\|_{L^2(J;H^{-1/2}(\Gamma_-))} + \|g_+\|_{L^2(J;H^{1/2}(\Gamma_+))})$$

Theorem 4.3
In addition to (4), assume that Ω is a convex polygonal domain and the coefficients $\mathbf{a}$, $\mathbf{b}$, c, f, and R satisfy

$$\mathbf{a} \in (W^{1,\infty}(\Omega_T))^{2\times 2}, \quad \mathbf{b} \in (W^{1,\infty}(\Omega_T))^2$$

$$\nabla \cdot \mathbf{b}, c \in W^{1,\infty}(\Omega_T), \quad f \in L^1(\Omega_T), \quad R \in L^\infty(J; W^{1,\infty}(\Omega))$$

If the solution $p, \mathbf{u}$ to (7) satisfies $p, \nabla \cdot \mathbf{u} \in C^1(J; H^1(\Omega))$ and $\mathbf{u} \in (C^1(J; H^1(\Omega)))^2$, and h and Δt are sufficiently small, then

$$\max_{1 \leqslant n \leqslant N} \|p^n - p_h^n\|_{L^2(\Omega)} + \left(\sum_{n=1}^{N} \|\mathbf{u}^n - \mathbf{u}_h^n\|_{\mathbf{L}^2(\Omega)}^2 \Delta t^n \right)^{1/2} \leqslant C(p, \mathbf{u})(h + \Delta t)$$

where $C(p, \mathbf{u}) > 0$ is independent of h and Δt:

$$C(p, \mathbf{u}) = C \left\{ \|p\|_{L^2(J;H^1(\Omega))} + \left\| \frac{\mathrm{d}p}{\mathrm{d}\tau} \right\|_{L^2(\Omega_T)} + \left\| \frac{\mathrm{d}}{\mathrm{d}\tau} \nabla \cdot \mathbf{u} \right\|_{L^2(\Omega_T)} + \left\| \frac{\partial \mathbf{u}}{\partial t} \right\|_{\mathbf{L}^2(J;\mathbf{H}^1(\Omega))} + \left\| \nabla \cdot \frac{\partial \mathbf{u}}{\partial t} \right\|_{L^2(J;H^1(\Omega))} + \|\mathbf{u}\|_{\mathbf{L}^\infty(J;\mathbf{H}^1(\Omega))} + \|\nabla \cdot \mathbf{u}\|_{L^\infty(J;H^1(\Omega))} + \|p_0\|_{H^1(\Omega)} \right\}$$

5. PROOF OF STABILITY AND CONVERGENCE

In this section, as an example, we carry out the proof of Theorems 2.2 and 2.3 for the MMOC-mixed covolume methods. The same results for the MMOCAA and Eulerian–Lagrangian mixed covolume

DOI: 10.1002/nla

methods can be shown by combining the present techniques and those in References [1, 6, 22] for studying these individual methods.

5.1. The proof of stability

The next lemma can be proven in a similar fashion as for Lemma 3.1 in Reference [35]. However, the assumption is weakened here. For the proof under the current assumption, see Lemma 3.4 in Reference [36].

Lemma 5.1
With assumption (12), for each n we have

$$(c\check{v}, \check{v}) - (cv, v) \leqslant C\Delta t^n (cv, v) \quad \forall v \in L^2(\Omega)$$

where $\check{v}(\mathbf{x}) = v(\mathbf{x} - \mathbf{b}(\mathbf{x}, t^n)\Delta t^n / c(\mathbf{x}))$.

Proof of Theorem 2.2
Take $w = p_h^n$ and $\mathbf{v} = \mathbf{u}_h^n$ in the first and second equations of (9), respectively, add the resulting two equations, multiply by Δt^n, use hypothesis (H1), and sum over n, $1 \leqslant n \leqslant N$, to see that

$$\sum_{n=1}^{N} (c(p_h^n - \check{p}_h^{n-1}), p_h^n) + \sum_{n=1}^{N} [((\mathbf{a}^n)^{-1}\mathbf{u}_h^n, \gamma_h \mathbf{u}_h^n) + (R^n p_h^n, p_h^n)]\Delta t^n = \sum_{n=1}^{N} (f^n, p_h^n)\Delta t^n \tag{32}$$

Note that

$$\begin{aligned}(c(p_h^n - \check{p}_h^{n-1}), p_h^n) &\geqslant \tfrac{1}{2}((cp_h^n, p_h^n) - (c\check{p}_h^{n-1}, \check{p}_h^{n-1})) \\ &= \tfrac{1}{2}\{((cp_h^n, p_h^n) - (cp_h^{n-1}, p_h^{n-1})) + ((cp_h^{n-1}, p_h^{n-1}) - (c\check{p}_h^{n-1}, \check{p}_h^{n-1}))\}\end{aligned}$$

so that Theorem 2.2 follows from (32), hypothesis (H2), Lemma 5.1, (4), and the discrete Gronwall inequality. □

5.2. The proof of convergence

5.2.1. Projection operators. In the derivation of error estimates for the standard mixed finite element methods, certain projection operators play an important role. The mixed covolume methods considered will also utilize similar projections.

On the reference rectangle $\hat{K} = [0, 1] \times [0, 1]$, the Raviart–Thomas projections $\hat{\mathbf{\Pi}} : (H^1(\hat{K}))^2 \to \mathbf{V}_h(\hat{K})$ and $\hat{P} : L^2(\hat{K}) \to W_h(\hat{K})$ are defined as follows:

$$\int_{\hat{e}} \hat{\mathbf{\Pi}}\hat{\mathbf{v}} \cdot \hat{\nu} \, \mathrm{d}\ell = \int_{\hat{e}} \hat{\mathbf{v}} \cdot \hat{\nu} \, \mathrm{d}\ell \quad \forall \hat{e} \in \partial\hat{K}$$

$$\int_{\hat{K}} \hat{P}\hat{w} \mathrm{d}\hat{\mathbf{x}} = \int_{\hat{K}} \hat{w} \mathrm{d}\hat{\mathbf{x}}$$

DOI: 10.1002/nla

For each quadrilateral $K \in K_h$, the projection $\mathbf{\Pi}_K : (H^1(K))^2 \to \mathbf{V}_h(K)$ and the map $P_K : L^2(K) \to W_h(K)$ are defined through the Piola transformation $\mathscr{P}_K$:

$$\mathbf{\Pi}_K \mathbf{v} = \mathscr{P}_K(\hat{\mathbf{\Pi}}\hat{\mathbf{v}}), \quad \mathbf{v} \in (H^1(K))^2$$

$$P_K w = (\hat{P}\hat{w}) \circ \mathbf{F}_K^{-1}, \quad w \in L^2(K)$$

where $\mathscr{P}_K \hat{\mathbf{v}} = \mathbf{v}$ and $\hat{w} = w \circ \mathbf{F}_K$. Finally, we define

$$\mathbf{\Pi}_h \mathbf{v}|_K = \mathbf{\Pi}_K \mathbf{v}, \quad P_h w|_K = P_K w$$

These two operators satisfy the orthogonal relations

$$\begin{aligned} &(\nabla \cdot (\mathbf{v} - \mathbf{\Pi}_h \mathbf{v}), v) = 0, \quad \mathbf{v} \in (H^1(\Omega))^2, \quad v \in W_h \\ &(\nabla \cdot \mathbf{w}, w - P_h w) = 0, \quad \mathbf{w} \in \mathbf{V}_h, \quad w \in W \end{aligned} \tag{33}$$

Moreover, they have the approximation properties [31]

$$\begin{aligned} \|\mathbf{v} - \mathbf{\Pi}_h \mathbf{v}\|_{\mathbf{L}^2(\Omega)} &\leqslant Ch \|\mathbf{v}\|_{\mathbf{H}^1(\Omega)}, \quad \mathbf{v} \in (H^1(\Omega))^2 \\ \|\nabla \cdot (\mathbf{v} - \mathbf{\Pi}_h \mathbf{v})\|_{L^2(\Omega)} &\leqslant Ch \|\nabla \cdot \mathbf{v}\|_{H^1(\Omega)}, \quad \mathbf{v} \in \mathbf{H}^1(\mathrm{div}, \Omega) \\ \|w - P_h w\|_{L^2(\Omega)} &\leqslant Ch \|w\|_{H^1(\Omega)}, \quad w \in H^1(\Omega) \end{aligned} \tag{34}$$

5.2.2. Proof of Theorem 2.3. To prove Theorem 2.3, we also need the next lemma [6].

Lemma 5.2
With assumption (12), for each n, if Δt^n is sufficiently small, we have

$$\|v^n - \check{v}\|_{L^2(\Omega)} \leqslant C(\Delta t^n)^{1/2} \left\| \frac{\partial v}{\partial \boldsymbol{\tau}} \right\|_{L^2(\Omega \times J^n)} \quad \forall v \in H^1(\Omega_T)$$

where $\check{v}(\mathbf{x}) = v(\mathbf{x} - \mathbf{b}(\mathbf{x}, t^n)\Delta t^n / c(\mathbf{x}))$.

Proof of Theorem 2.3
Subtract (9) from (6) with $t = t^n$ and use (H1) to have the error equations

$$\begin{aligned} &\left(\psi^n \frac{\partial p^n}{\partial \boldsymbol{\tau}} - c \frac{p_h^n - \check{p}_h^{n-1}}{\Delta t^n}, w \right) + (\nabla \cdot [\mathbf{u}^n - \mathbf{u}_h^n], w) + (R^n[p^n - p_h^n], w) = 0, \quad w \in W_h, \\ &((\mathbf{a}^n)^{-1}\mathbf{u}^n, \mathbf{v} - \gamma_h \mathbf{v}) + ((\mathbf{a}^n)^{-1}[\mathbf{u}^n - \mathbf{u}_h^n], \gamma_h \mathbf{v}) - (\nabla \cdot \mathbf{v}, p^n - p_h^n) = 0, \quad \mathbf{v} \in \mathbf{V}_h \end{aligned} \tag{35}$$

Choose $\mathbf{v} = \mathbf{\Pi}_h(\mathbf{u}^n - \mathbf{u}_h^n)$ and $w = P_h(p^n - p_h^n)$, add the resulting equations, and use the orthogonal relations (33) to give

$$\begin{aligned} &\left(\psi^n \frac{\partial p^n}{\partial \boldsymbol{\tau}} - c \frac{p_h^n - \check{p}_h^{n-1}}{\Delta t^n}, P_h(p^n - p_h^n) \right) + (R^n[p^n - p_h^n], P_h(p^n - p_h^n)) \\ &\quad + ((\mathbf{a}^n)^{-1}\mathbf{u}^n, \mathbf{\Pi}_h(\mathbf{u}^n - \mathbf{u}_h^n) - \gamma_h \mathbf{\Pi}_h(\mathbf{u}^n - \mathbf{u}_h^n)) \\ &\quad + ((\mathbf{a}^n)^{-1}[\mathbf{u}^n - \mathbf{u}_h^n], \gamma_h \mathbf{\Pi}_h(\mathbf{u}^n - \mathbf{u}_h^n)) = 0 \end{aligned} \tag{36}$$

DOI: 10.1002/nla

We bound each term in (36). For this, set

$$\boldsymbol{\eta}_1^n = \boldsymbol{\Pi}_h \mathbf{u}^n - \mathbf{u}_h^n, \quad \boldsymbol{\eta}_2^n = \boldsymbol{\Pi}_h \mathbf{u}^n - \mathbf{u}^n, \quad \zeta_1^n = P_h p^n - p_h^n, \quad \zeta_2^n = P_h p^n - p^n$$

so $\mathbf{u}^n - \mathbf{u}_h^n = \boldsymbol{\eta}_1^n - \boldsymbol{\eta}_2^n$ and $p^n - p_h^n = \zeta_1^n - \zeta_2^n$. With these notation, Equation (36) is rewritten as

$$\left(\psi^n \frac{\partial p^n}{\partial \boldsymbol{\tau}} - c\frac{p_h^n - \check{p}_h^{n-1}}{\Delta t^n}, \zeta_1^n\right) + ((\mathbf{a}^n)^{-1}\boldsymbol{\eta}_1^n, \gamma_h \boldsymbol{\eta}_1^n) + (R^n \zeta_1^n, \zeta_1^n)$$

$$= ((\mathbf{a}^n)^{-1}\boldsymbol{\eta}_2^n, \gamma_h \boldsymbol{\eta}_1^n) + (R^n \zeta_2^n, \zeta_1^n) - ((\mathbf{a}^n)^{-1}\mathbf{u}^n, \boldsymbol{\eta}_1^n - \gamma_h \boldsymbol{\eta}_1^n) \tag{37}$$

Below ε is a positive constant independent of h, as small as we please. It follows from (4b) and (16) that

$$|((\mathbf{a}^n)^{-1}\boldsymbol{\eta}_2^n, \gamma_h \boldsymbol{\eta}_1^n)| \leqslant C\|\boldsymbol{\eta}_2^n\|^2_{\mathbf{L}^2(\Omega)} + \varepsilon\|\boldsymbol{\eta}_1^n\|^2_{\mathbf{L}^2(\Omega)} \tag{38}$$

Next, it is obvious that

$$|(R^n \zeta_2^n, \zeta_1^n)| \leqslant C(\|\zeta_2^n\|_{L^2(\Omega)} + \|\zeta_1^n\|_{L^2(\Omega)}) \tag{39}$$

Also, using (17), we see that

$$|((\mathbf{a}^n)^{-1}\mathbf{u}^n, \boldsymbol{\eta}_1^n - \gamma_h \boldsymbol{\eta}_1^n)| \leqslant Ch\|\mathbf{u}^n\|^2_{\mathbf{H}^1(\Omega)} + \varepsilon\|\boldsymbol{\eta}_1^n\|^2_{\mathbf{L}^2(\Omega)} \tag{40}$$

Now, observe that

$$\left(\psi^n \frac{\partial p^n}{\partial \boldsymbol{\tau}} - c\frac{p_h^n - \check{p}_h^{n-1}}{\Delta t^n}, \zeta_1^n\right)$$

$$= \left(c\frac{\zeta_1^n - \check{\zeta}_1^{n-1}}{\Delta t^n}, \zeta_1^n\right) + \left(\psi^n \frac{\partial p^n}{\partial \boldsymbol{\tau}} - c\frac{p^n - \check{p}^{n-1}}{\Delta t^n}, \zeta_1^n\right) - \left(c\frac{\zeta_2^n - \check{\zeta}_2^{n-1}}{\Delta t^n}, \zeta_1^n\right)$$

By Lemma 5.1, we have

$$\left(c\frac{\zeta_1^n - \check{\zeta}_1^{n-1}}{\Delta t^n}, \zeta_1^n\right) \geqslant \frac{1}{2\Delta t^n}((c\zeta_1^n, \zeta_1^n) - (c\check{\zeta}_1^{n-1}, \check{\zeta}_1^{n-1}))$$

$$\geqslant \frac{1}{2\Delta t^n}((c\zeta_1^n, \zeta_1^n) - (c\zeta_1^{n-1}, \zeta_1^{n-1})) - C(c\zeta_1^{n-1}, \zeta_1^{n-1}) \tag{41}$$

Using a standard backward difference error analysis [10], we see that

$$\left|\left(\psi^n \frac{\partial p^n}{\partial \boldsymbol{\tau}} - c\frac{p^n - \check{p}^{n-1}}{\Delta t^n}, \zeta_1^n\right)\right| \leqslant C\left(\sum_{K \in K_h} \left\|\frac{\partial^2 p}{\partial \boldsymbol{\tau}^2}\right\|^2_{L^2(K \times J^n)} \Delta t^n + \|\zeta_1^n\|^2_{L^2(\Omega)}\right) \tag{42}$$

DOI: 10.1002/nla

We write

$$\left(c\frac{\zeta_2^n-\check{\zeta}_2^{n-1}}{\Delta t^n},\zeta_1^n\right)=\left(c\frac{\zeta_2^n-\zeta_2^{n-1}}{\Delta t^n},\zeta_1^n\right)+\left(c\frac{\zeta_2^{n-1}-\check{\zeta}_2^{n-1}}{\Delta t^n},\zeta_1^n\right)$$

consequently, by Lemma 5.2, we find that

$$\begin{aligned}\left|\left(c\frac{\zeta_2^n-\zeta_2^{n-1}}{\Delta t^n},\zeta_1^n\right)\right|&\leqslant C\left(\|\zeta_1^n\|^2_{L^2(\Omega)}+\frac{1}{\Delta t^n}\left\|\frac{\partial\zeta_2}{\partial t}\right\|^2_{L^2(\Omega\times J^n)}\right)\\ \left|\left(c\frac{\zeta_2^{n-1}-\check{\zeta}_2^{n-1}}{\Delta t^n},\zeta_1^n\right)\right|&\leqslant C\left(\|\zeta_1^n\|^2_{L^2(\Omega)}+\frac{1}{\Delta t^n}\left\|\frac{\partial\zeta_2}{\partial\boldsymbol{\tau}}\right\|^2_{L^2(\Omega\times J^{n-1})}\right)\end{aligned}\tag{43}$$

Finally, substitute (38)–(43) into (37), multiply by Δt^n, sum over n from 1 to N, and use (4), (H2), (34), the triangle inequality, and the discrete Gronwall inequality to complete the proof of Theorem 2.3. □

REFERENCES

1. Chen Z. *Finite Element Methods and Their Applications*. Springer: Heidelberg, New York, 2005.
2. Barrett JW, Morton KW. Approximate symmetrization and Petrov–Galerkin methods for diffusion-convection problems. *Computer Methods in Applied Mechanics and Engineering* 1984; **45**:97–122.
3. Brooks A, Hughes TJ. Streamline upwind Petrov–Galerkin formulations for convection dominated flows with particular emphasis on the incompressible Navier–Stokes equations. *Computer Methods in Applied Mechanics and Engineering* 1982; **32**:199–259.
4. Christie I, Griffiths DF, Mitchell AR. Finite element methods for second order differential equations with significant first derivatives. *International Journal for Numerical Methods in Engineering* 1976; **10**:1389–1396.
5. Westerink JJ, Shea D. Consistent higher degree Petrov–Galerkin methods for the solution of the transient convection-diffusion equation. *International Journal for Numerical Methods in Engineering* 1989; **13**:839–941.
6. Arbogast T, Wheeler MF. A characteristics-mixed finite element for advection-dominated transport problems. *SIAM Journal on Numerical Analysis* 1995; **32**:404–424.
7. Celia MA, Russell TF, Herrera I, Ewing RE. An Eulerian–Lagrangian localized adjoint method for the advection-diffusion equation. *Advances in Water Resources* 1990; **13**:187–206.
8. Chen Z. Characteristic mixed discontinuous finite element methods for advection-dominated diffusion problems. *Computer Methods in Applied Mechanics and Engineering* 2002; **191**:2509–2538.
9. Chen Z. Characteristic-nonconforming finite element methods for advection-dominated diffusion problems. *Computers and Mathematics with Applications* 2004; **48**:1087–1100.
10. Douglas Jr J, Russell TF. Numerical methods for convection dominated diffusion problems based on combining the method of characteristics with finite element or finite difference procedures. *SIAM Journal on Numerical Analysis* 1982; **19**:871–885.
11. Brezzi F, Fortin M. *Mixed and Hybrid Finite Element Methods*. Springer: New York, 1991.
12. Chou SH, Kwak DY, Kim KY. Mixed finite volume methods on nonstaggered quadrilateral grids for elliptic problems. *Mathematics of Computation* 2003; **72**:525–539.
13. Cai Z, Jones JE, McCormick SF, Russell TF. Control-volume mixed finite element methods. *Computational Geosciences* 1997; **1**:289–315.
14. Chou SH, Kwak DY. Mixed covolume methods on rectangular grids for elliptic problems. *SIAM Journal on Numerical Analysis* 1997; **37**:85–104.
15. Chou SH, Kwak DY, Vassilevski PS. Mixed upwinding covolume methods on rectangular grids for convection-diffusion problems. *SIAM Journal on Scientific and Statistical Computing* 1999; **21**:145–165.
16. Lazarov RD, Mishev ID, Vassilevski PS. Finite volume methods for convection-diffusion problems. *SIAM Journal on Numerical Analysis* 1996; **33**:31–55.

DOI: 10.1002/nla

17. Russell TF. Rigorous block-centered discretization on irregular grids: improved simulation of complex reservoir systems. *Technical Report 3*, Reservoir Research Corporation, Tulsa, OK, 1995.
18. Cavendish JC, Hall CA, Porsching TA. A complementary volume approach for modeling three-dimensional Navier–Stokes equations using dual Delaunay/Voronoi tessellations. *International Journal of Numerical Methods for Heat and Fluid Flow* 1994; **4**:239–345.
19. Nicolaides RA, Porsching TA, Hall CA. Covolume methods in computational fluid dynamics. In *Computational Fluid Dynamics Review*, Hafez M, Oshma K (eds). Wiley: New York, 1995; 279–299.
20. Chou SH. Analysis and convergence of a covolume method for the generalized Stokes problem. *Mathematics of Computation* 1997; **66**:85–104.
21. Pironneau O. On the transport-diffusion algorithm and its application to the Navier–Stokes equations. *Numerische Mathematik* 1982; **38**:309–332.
22. Douglas Jr J, Furtado F, Pereira F. On the numerical simulation of water flooding of heterogeneous petroleum reservoirs. *Computational Geosciences* 1997; **1**:155–190.
23. Brezzi F, Douglas Jr J, Durán R, Fortin M. Mixed finite elements for second order elliptic problems in three variables. *Numerische Mathematik* 1987; **51**: 237–250.
24. Brezzi F, Douglas Jr J, Fortin M, Marini LD. Efficient rectangular mixed finite elements in two and three space variables. *RAIRO-Mathematical Modelling and Numerical Analysis-Modelisation* 1987; **21**:581–604.
25. Brezzi F, Douglas Jr J, Marini LD. Two families of mixed finite elements for second order elliptic problems, *Numerische Mathematik* 1985; **47**:217–235.
26. Chen Z, Douglas Jr J. Prismatic mixed finite elements for second order elliptic problems. *Calcolo* 1989; **26**:135–148.
27. Nédélec JC. A new family of mixed finite elements in $\mathbb{R}^3$. *Numerische Mathematik* 1986; **50**:57–81.
28. Raviart R, Thomas J-M. *A Mixed Finite Element Method for Second Order Elliptic Problems*. Lecture Notes in Mathematics, vol. 606. Springer: Berlin, 1977; 292–315.
29. Chou SH, Vassilevski PS. A general mixed covolume framework for constructing conservative schemes for elliptic problems. *Mathematics of Computation* 1999; **68**:991–1011.
30. Harlow FH, Welch FE. Numerical calculations of time dependent viscous incompressible flow of fluid with a free surface. *Physics of Fluids* 1995; **8**:2181–2197.
31. Chou SH, Kwak DY, Kim KY. A general framework for constructing and analyzing mixed finite volume methods on quadrilateral grids: the overlapping covolume case. *SIAM Journal on Numerical Analysis* 2001; **39**:1170–1196.
32. Arnold DN, Boffi D, Falk R. Quadrilateral $H(\mathrm{div})$ finite elements. *SIAM Journal on Numerical Analysis* 2005; **42**:2429–2451.
33. Wang J, Mathew T. Mixed finite element methods over quadrilaterals. In *Proceedings of the Third International Conference on Advances in Numerical Methods and Applications*, Dimov IT *et al.* (eds). World Scientific: Singapore, 1994; 203–214.
34. Chen Z, Huan G, Ma Y. *Computational Methods for Multiphase Flows in Porous Media*. Computational Science and Engineering Series, vol. 2. SIAM: Philadelphia, PA, 2006.
35. Dawson CN, Russell TF, Wheeler MF. Some improved error estimates for the modified method of characteristics. *SIAM Journal on Numerical Analysis* 1989; **26**:1487–1512.
36. Chen Z, Ewing RE, Jiang EQ, Spagnuolo AM. Error analysis for characteristics-based methods for degenerate parabolic problems. *SIAM Journal on Numerical Analysis* 2002; **40**:1491–1515.

DOI: 10.1002/nla